Time-Temperature Superposition Based Accelerated Aging Method for Packaged MEMS Resonators

Jeronimo Segovia-Fernandez[1], Enis Tuncer[2], Sean Chang[1], Ernest Ting-Ta Yen[1]
[1]Kilby Labs / [2]SCP
Texas Instruments
[1]Santa Clara, CA / [2]Dallas, TX
jeronimo.segovia@ti.com

***Summary*—This manuscript introduces a new methodology to accelerate and predict stress-related aging in encapsulated MEMS resonators. This approach builds upon the time-temperature superposition principle that, in linear viscoelastic materials, relates the relaxation modulus ($E(t,T)$) at low temperature with the one measured at high temperature for a shorter range of time. The master curve shift factors derived from this correspondence permit us to reconstruct $E(t,T)$ at room conditions from a relaxation profile that shrinks as a consequence of applying a staircase-like temperature. Thence, we use this technique to accelerate the aging of a MEMS resonator whose frequency is affected by package relaxation and, with the semi-analytical equation introduced in this manuscript, calculate the long-term drift. To validate this approach, a 4-step temperature function in log time scale is applied to a thickness-extensional MEMS resonator known as DBAR that is surrounded by mold compound in a QFN package.**

Keywords— MEMS aging; dynamic mechanical analysis; time-temperature superposition; thermal-stress FEM.

I. Introduction

Frequency stability can be classified into short-term, which is usually measured at rates <1s and has a random nature (*i.e.* amplifier flicker noise), and long-term, which is relatively slower and has a deterministic nature [1]. Among the causes of long-term drifts, commercial MEMS resonators have demonstrated low vibration and shock sensitivities [2], supply voltage regulation by means of on-chip LDOs [3], and vacuum sealed encapsulation against particles, humidity, gases, etc. [4]. Moreover, temperature compensation and ovenization have minimized the influence of ambient temperature on the MEMS resonance frequency (f_r) [5], [6]. However, these circuit techniques cannot correct for the temperature gradients that exist between molding and assembly steps inducing non-uniform thermal deformations inside the package. Due to the forming viscoelastic epoxies (especially mold compound), the built-up stress generates aging.

Typical aging requirements are application-dependent and, for timing solutions, can range from tens of ppm (*i.e.* local-area wireless standards [7]) to less than one ppm (*i.e.* LTE communications [8]). Qualifying a quartz crystal or a MEMS resonator for a specific application requires measuring the relative frequency shift through the entire life of the product, typically 10 years. Since this is impractical, accelerated aging involving measurement at greater temperatures (T) has been proposed as an alternative procedure. Following military standards [9], the parts are heated up to 85°C for 30 days and 105°C for 168h as an equivalent of one year at 25°C. By using an Arrhenius model, the measured drift is fitted for every T to extract the activation energy [10]. However, this technique: 1) requires fitting a logarithmic function, which does not match with the entire aging profile, 2) exhibits several downtimes, since the oven needs to be readjusted for every T, and 3) does not discriminate among different sources of aging, the model is purely experimental and not based on a physical phenomenon.

In this work, we introduce a new accelerated aging methodology based on time-temperature superposition to predict the effect of package stress relaxation on the f_r of MEMS resonators. In linear viscoelastic materials, time-temperature superposition establishes that, for every T, the $E(t,T)$ shifts a specific time interval. Under this principle, a multi-step temperature function can be applied and its effect on $E(t,T)$ extrapolated to any constant T. In this paper, we apply a 4-step temperature function in log time scale that allows us to predict the frequency drift of a QFN-encapsulated, thickness-extensional, piezoelectric MEMS resonator known as DBAR (Dual-Bragg Acoustic Resonator) [11]. By normalizing over T and re-scaling the time axis, we prove via FEM that we can extrapolate the results to aging at 35°C.

II. Dynamic Mechanical Analysis (DMA)

To determine the viscoelastic behavior of mold compound we run DMA. This technique allows us to differentiate between the storage and loss moduli by applying a sinusoidal force and measuring the in-phase (elastic) and out-of-phase (viscous) deformations. For this work, we tested the Sumitomo G700LTD, a halogen free/high reliability epoxy resin often used in QFN packaging. After curing, this thermosetting material was subjected to a sinusoidal load of 3N perpendicular to a two-point clamped specimen and a frequency sweep from 1 to 20Hz. In addition, the deformation rate depends on temperature, becoming more pronounced above glass transition (T_g). To find T_g, we swept the temperature from room temperature to 200°C. Fig. 1 plots the storage and loss moduli computed by our DMA instrument (TA Q800). By selecting the segment corresponding to the peak of loss modulus, we find that T_g=83°C.

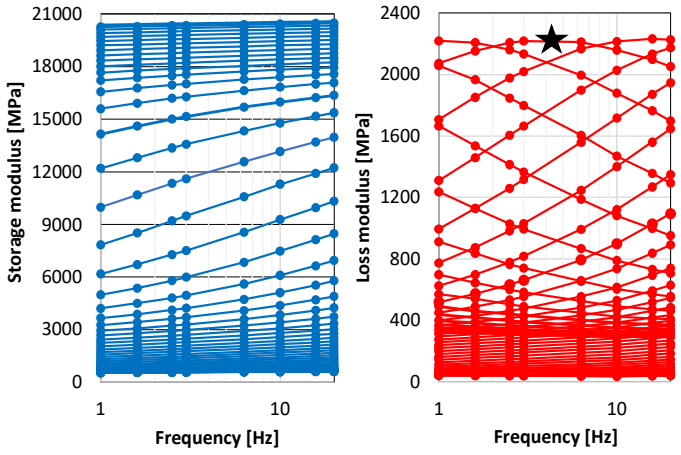

Fig. 1: Storage and loss moduli of G700LTD generated via DMA across temperatures and frequencies. The "star" symbol on the loss modulus marks the T_g curve.

Time-temperature superposition stablishes that linear viscoelastic materials exhibit the same shape of complex modulus in both time and temperature domains. Under this principle, we can recreate the storage and loss moduli by shifting horizontally the DMA segments until they align over a broader frequency spectrum. The outcome of this curve reconstruction is the master curve, which contains the time-temperature shift factors ($a_T(T)$) and quantifies how much the $E(t,T)$ shifts for every T (for example, relaxation shifts to the left when $a_T(T)<1$ and to the right when $a_T(T)>1$). Different analytical models can be used to generate the $a_T(T)$ in linear polymers [12]. For G700LTD, we use the Arrhenius law, which provides relatively smooth profiles for both storage and loss moduli.

$$\log a_T(T) = -\frac{E_a}{2.303R}\left(\frac{1}{T}-\frac{1}{T_{ref}}\right) \quad (1)$$

where E_a, R, and T_{ref} stand for activation energy, universal gas constant and reference temperature, respectively. The best alignment of DMA curves is obtained when E_a=-3.8e5J/mol and T_{ref}=310K.

III. Relaxation Modulus

The $E(t,T)$ describes the rate of stress relaxation over time and temperature. This magnitude is computed as the absolute value of the storage (real) and loss (imaginary) moduli while time is calculated as the inverse of load frequency. In most linear viscoelastic materials, relaxation does not occur at a single time (molecular segments of different lengths have different relaxation times). To account for multiple relaxations, typical $E(t,T)$ models rely on a finite sum of exponential terms known as Prony Series (PS). For example, the Generalized Maxwell model, which combines several dashpot (η_i)-spring (E_i) branches in parallel and has a temperature-dependent time constant per branch ($\tau_i(T)$) equal to η_i/E_i, can be expressed with the following PS in time domain:

$$E(t,T) = E_\infty + \sum_{i=1}^{N} E_i \exp -(t/\tau_i(T)) \quad (2)$$

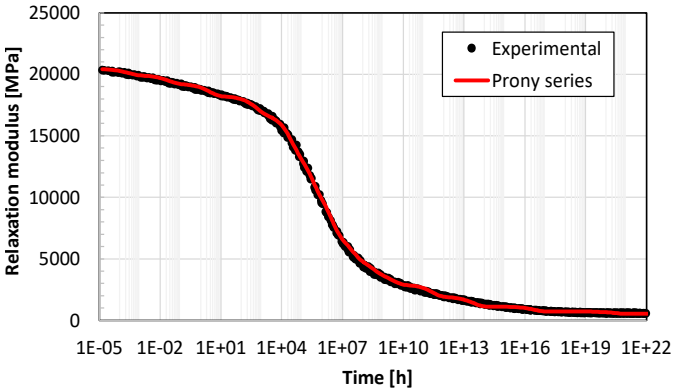

Fig. 2: Measured and fitted $E(t,T)$ of mold compound at 310K.

TABLE I: G700LTD RELAXATION CONSTANTS. E_∞=525MPa

	i=1	i=2	i=3	i=4	i=5	i=6	i=7	i=8	i=9	i=10	i=11	i=12	i=13	i=14
$\tau_{ref,i}$ [s]	1	1e2	1e4	2e6	1e8	1e9	1e10	1e11	1e12	1e13	1e15	1e17	1e20	1e24
E_i [MPa]	500	700	1000	1400	2800	3100	3800	2000	1200	1000	1000	800	400	200

Fig. 2 plots both experimental and fitted $E(t,T_{ref})$ of G700LTD. For the fitting, we employ a PS of 14 relaxation modes, whose values are contained in Table I.

IV. Multi-Step Temperature Function

At low temperature, stress relaxation occurs at slow rate. For example, at 310K, G700LTD requires 10^{16} h to fully relax (see Fig. 2). To speed up relaxation, temperature can be increased ($a_T(T)<1$ when $T>T_{ref}$, so $E(t,T)$ shifts to left). However, if temperature increases too quickly those relaxation modes with $\tau_{ref,i}\cdot a_T(T)$ below the measurement speed will not be recorded. For example, if T=365K then $a_T(T)$=4.15e-11 based on (1). As a result, the largest relaxation mode in the PS (E_7=3,800MPa) will exhibit a $\tau_{ref,7}\cdot a_T(T)<1$s. For that reason, it is advised to gradually increase temperature and, to achieve that, a staircase-like temperature function can be implemented. To analyze the effect of temperature on our mold compound, the transient response of a hypothetical 10x1mm^2 slab subjected to a fixed axial displacement u_x=-0.1mm is simulated in COMSOL Multiphysics (Fig. 3).

To cover the entire relaxation of G700LTD, we select a 4-step function in which T is equal to 35°C when t<1h, 60°C when 1h<t<10h, 85°C when 10h<t<100h, and 105°C when t>100h. Fig. 4 plots the resulting $E(t,T)$ (simulated as the axial stress over axial strain in the center of the slab) as well as the relaxation curves corresponding to each specific T. On Fig. 4 we can notice that, at temperature transitions, $E(t,T)$ "jumps" from one curve to another, exhibiting an exponential decay.

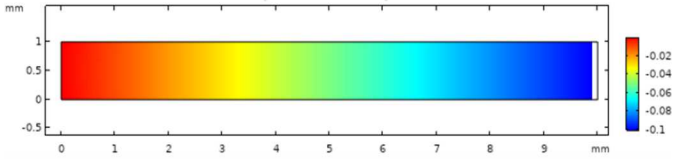

Fig. 3: Simulated 10x1mm^2 G700LTD slab anchored on the left and subjected to a fixed -0.1mm displacement on the right.

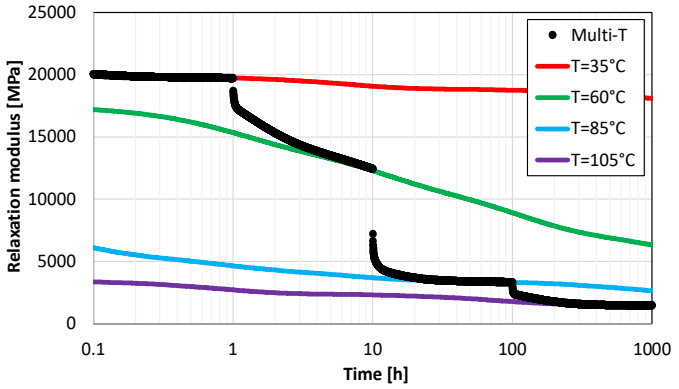

Fig. 4: Accelerated $E(t,T)$ resulting from the 4-step temperature function (dotted line) and long-term $E(t,T)$ corresponding to each of the function temperatures (solid lines).

To recreate the relaxation profile at a constant T, we follow the time-temperature superposition principle. Instead of multiplying the relaxation constants by $a_T(T)$, we rescale the time axis by dividing the actual time over $a_T(T)$. As a result, the new time axis (*a.k.a.* effective time) is shifted towards larger numbers when temperature goes up and smaller numbers when temperature goes down. For time-dependent temperatures ($T(t)$), $a_T(T)$ becomes an implicit function of time. Assuming a continuous time function, the effective time (t') can be calculated as follows [13]:

$$t' = \int_0^t \frac{dt}{a_T(T(t))} \tag{3}$$

By combining (1) and (3), we can recreate the $E(t,T)$ of G700LTD at any temperature from the multi-step data outlined on Fig. 4. Indeed, Fig. 5 shows that the $E(t,T_{ref})$ based on (2) overlaps the $E'(t,T_{ref})$ recreated from the multi-step data at the same temperature. Fundamentally, we can infer from this graph that, when the temperature changes at a faster rate than the viscoelastic material relaxes (see the $E(t,T)$ jumps), the time axis "stretches", creating clusters of data points. A more continuous relaxation curve could be achieved by applying a smaller time step.

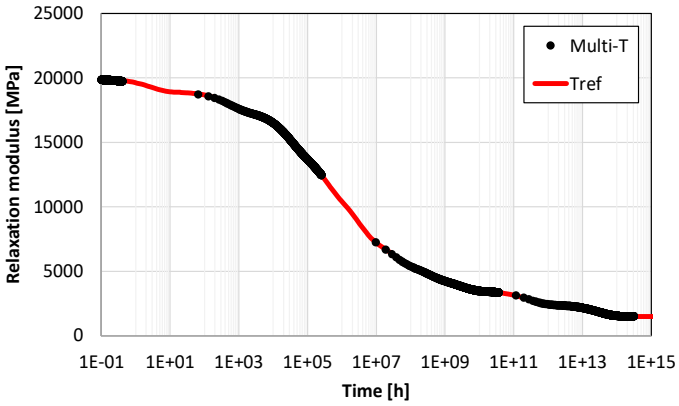

Fig. 5: $E(t,T)$ of mold compound simulated at T_{ref}=35°C and recreated from 4-step temperature data after applying the time-temperature superposition formulas.

V. Accelerated Aging

Commercial MEMS require plastic encapsulation which, in the case of resonators, may induce frequency drift due to stress relaxation. In this paper, we correlate the frequency drift of a DBAR with mold compound relaxation through the evolution of its vertical strain ($\varepsilon_z(t,T)$). The DBAR exhibits a thickness-extensional mode that makes its f_r to be inversely proportional to the thickness of the piezoelectric film [11]. Assuming that this magnitude varies at a rate equal to $\varepsilon_z(t,T)$, the new resonance frequency will be inversely proportional to $1+\varepsilon_z(t,T)$ which results in the following relative drift [14]:

$$\frac{f_r(t,T) - f_{r0}}{f_{r0}}[ppm] = \left(\frac{1+\varepsilon_{z0}}{1+\varepsilon_z(t,T)} - 1\right)10^6 \tag{4}$$

where the sub-index 0 represents initial values.

For this study, a 6-pin QFN package is used to encapsulate the DBAR with an IC die that measures its frequency drift (Fig. 6). The FEM assumes that mold compound becomes so soft at soldering ($E \sim E_\infty$) that no stress is applied on the DBAR. Under this condition, we set the soldering temperature (180°C) as the thermal-stress equilibrium point. Moreover, the bottom side of metal solders are treated as fixed constraints. Fig. 7 plots the temperature of study following the 4-step function as well as the corresponding frequency drift of DBAR.

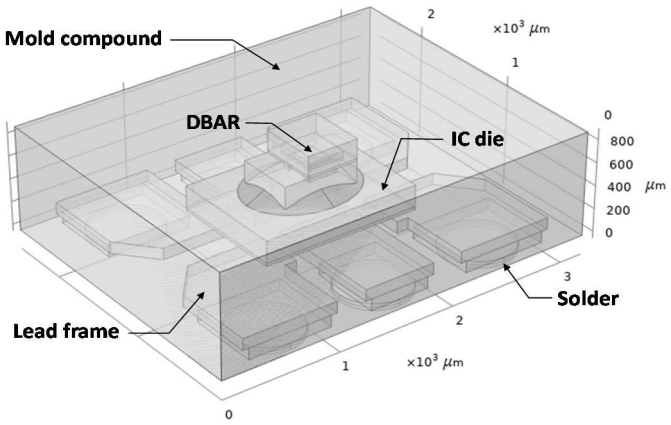

Fig. 6: Simulated QFN package containing DBAR and IC dies.

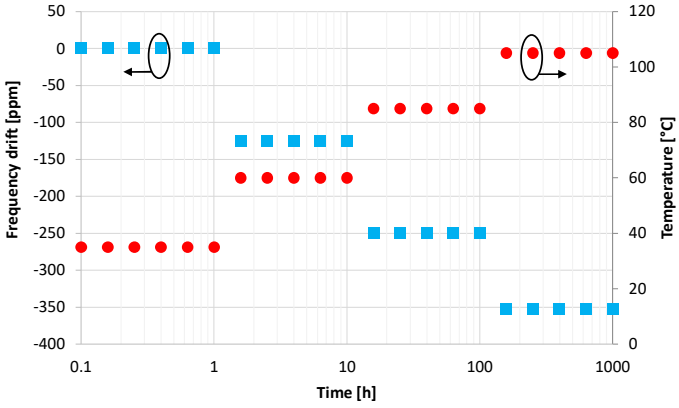

Fig. 7: 4-step temperature and frequency drift of DBAR. The FEM includes thermal deformation and G700LTD relaxation modulus.

Aging is defined as the relative frequency drift with time when external factors are maintained constant. However, the difference that exist between real-time and initial temperatures generate frequency jumps (see Fig. 7). To convert from the multi-step frequency drift to aging, we need to multiply $\varepsilon_z(t,T)$ by the ratio of initial and real-time temperature gradients.

$$\frac{f_r'(t)-f_{r0}}{f_{r0}}[ppm]=\left(\frac{1+\varepsilon_{z0}}{1+\frac{\varepsilon_z(t,T)(T_0-T_{eq})}{T(t)-T_{eq}}}-1\right)10^6 \quad (5)$$

where T_{eq} represents the equilibrium temperature at soldering, T_0 represents the initial temperature at which ε_{z0} is computed and $T(t)$ represents the real-time temperature.

Although (5) can be applied in simulations, experimentally we need to replace the $\varepsilon_z(t,T)$ by a known magnitude. In that case, we can use the original frequency drift (our measured signal) and combine (4) and (5) to obtain the following expression:

$$\frac{\Delta f_r'}{f_{r0}}=\frac{\frac{\Delta f_r}{f_{r0}}+1+\left(\frac{\Delta f_r}{f_{r0}}+1\right)\varepsilon_{z0}}{\left(1-\frac{T_0-T_{eq}}{T(t)-T_{eq}}\right)\frac{\Delta f_r}{f_{r0}}+\frac{T_0-T_{eq}}{T(t)-T_{eq}}\varepsilon_{z0}+1}-1 \quad (6)$$

where $\Delta f_r=f_r(t,T)-f_{r0}$ and $\Delta f_r'=f_r'(t)-f_{r0}$. From (6) it is important to point out that there will be two constants (T_0 and T_{eq}), whose values can be deduced experimentally, and one fitting parameter (ε_{z0}).

In addition to temperature normalization, we need to account for the shift in relaxation time constants that mold compound exhibits when subjected to multiple temperatures. Similar to what we did to recreate $E'(t,T_{ref})$ from the multi-step function (see Fig. 5), we can replace the time axis by the effective time based on (3). Fig. 8 compares the aging that results from frequency drift conversion using (6) and time re-scaling vs. the one simulated at T_{ref}. Although the square markers become dispersed (due to limited computational memory), both curves show identical trends. This validates our methodology and the use of a staircase-like temperature function to accelerate aging. As a final remark, the proposed approach allows us to compute aging at any temperature by simply changing T_{ref} in (1).

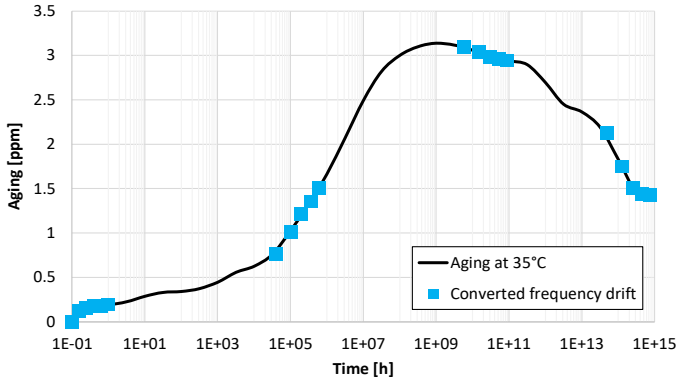

Fig. 8: DBAR aging at 35°C based on simulations at constant temperature and multi-step frequency drift conversion.

VI. Conclusions

An accelerated aging methodology to predict frequency drift due to package stress relaxation in MEMS resonators has been introduced. This approach is built upon the time-temperature superposition principle that, in linear viscoelastic materials, establishes a correlation between the rate of relaxation and temperature. Therefore, we propose to expose the MEMS resonators to a multi-step temperature in the log time scale (this gradually accelerates package relaxation) and extrapolate the 10-year aging curve from the frequency drift (this implies setting initial and equilibrium temperatures, and fitting the initial vertical strain until achieving a smooth profile). The proposed approach is validated via FEM by applying a 4-step temperature to a QFN-encapsulated DBAR whose f_r is affected by thermally-induced deformation and mold compound relaxation.

References

[1] R. Wojtyna, "Long-term and short-term frequency stabilities in sinusoidal oscillators," in *IEEE International Symposium on Circuits and Systems*, Jun. 1988, pp. 639–641.

[2] B. Kim, R. H. Olsson, K. Smart, and K. E. Wojciechowski, "MEMS resonators with extremely low vibration and shock sensitivity," in *2011 IEEE SENSORS*, Oct. 2011, pp. 606–609.

[3] R. J. Milliken, J. Silva-Martinez, and E. Sanchez-Sinencio, "Full On-Chip CMOS Low-Dropout Voltage Regulator," *IEEE Transactions on Circuits and Systems I: Regular Papers*, vol. 54, no. 9, pp. 1879–1890, Sep. 2007.

[4] B. Kim, R. N. Candler, M. Hopcroft, M. Agarwal, W.-T. Park, and T. W. Kenny, "Frequency stability of wafer-scale encapsulated MEMS resonators," in *TRANSDUCERS*, Jun. 2005, pp. 1965–1968.

[5] M. Heidarpour Roshan *et al.*, "A MEMS-Assisted Temperature Sensor With 20-µK Resolution, Conversion Rate of 200 S/s, and FOM of 0.04 pJK2," *IEEE Journal of Solid-State Circuits*, vol. 52, no. 1, pp. 185–197, 2017.

[6] J. Koo, K. Sankaragomathi, R. Ruby, and B. Otis, "A ±1.55ppm Stable FBAR Reference Clock with Oven-Controlled Temperature Compensation," *Journal of Electrical and Computer Engineering*, vol. 2018, p. e5453432, 2018.

[7] "IEEE, Standard 802.15.4."

[8] "ETSI Technical Specification 136 106."

[9] "MIL-PRF-3098."

[10] S. Wang *et al.*, "Aging models and parameters of quartz crystal resonators and oscillators," in *SPAWDA*, Oct. 2015, pp. 382–385.

[11] E. T.-T. Yen *et al.*, "Integrated High-frequency Reference Clock Systems Utilizing Mirror-encapsulated BAW Resonators," in *IEEE IUS*, Oct. 2019, pp. 2174–2177.

[12] A. Plota and A. Masek, "Lifetime Prediction Methods for Degradable Polymeric Materials—A Short Review," *Materials*, vol. 13, no. 20, Art. no. 20, Jan. 2020.

[13] W. N. Findley, J. S. Lai, and K. Onaran, *Creep And Relaxation Of Nonlinear Viscoelastic Materials With An Introduction To Linear Viscoelasticity*. North Holland, 2012.

[14] J. Segovia-Fernandez, E. T.-T. Yen, J. Rojas, T. Tran, M. Chowdhury, and P. Smeys, "An Analytical Model to Predict Extrinsic Aging in BAW Resonators," in *IEEE IFCS*, Jul. 2020, pp. 1–14.